

Quantum cascade laser gain medium modeling using a second-nearest neighbor sp^3s^* tight-binding model

Jeremy Green, Timothy B. Boykin, Corrie D. Farmer, Michel Garcia, Charles N. Ironside, *Member, IEEE*, Gerhard Klimeck, *Member, IEEE*, Roger Lake, *Senior Member, IEEE*, and Colin R. Stanley, *Member, IEEE*

Abstract—A ten-band sp^3s^* second-nearest neighbor tight-binding model has been used to model the electronic structure of various $\text{Al}_x\text{Ga}_{1-x}\text{As}$ quantum cascade laser gain media. The results of the simulations have been compared with experimental emission wavelength data, and it has been shown that the model is able to predict bounds on the photon energy at the peak in the gain coefficient spectrum to within at worst 21% of the experimental value. It is believed that the accuracy of the predictions can be improved by better analysis of the electronic structures. Comparison of the results of the calculations with results from a two-band $k \cdot p$ model shows that the tight-binding model is able to find the X -like states simultaneously with the Γ -like states. Two methods have been used to estimate the electric field at laser threshold and it is found that neither method offered any substantial advantage over the other. The effects of increasing and decreasing all the layer thicknesses in the gain medium by one monolayer have also been investigated.

Index Terms—Quantum cascade laser, tight-binding, second-nearest neighbor, intersubband, NEMO, gas sensing, gas detection.

I. INTRODUCTION

THE quantum cascade laser (QCL) is an electrically pumped semiconductor laser that emits in the mid-infrared region of the electromagnetic spectrum. Unlike most semiconductor injection lasers, which use electron-hole recombination to generate gain, the QCL is unipolar and light emission takes place when electrons undergo transitions between confinement-induced energy levels in just one band. The first demonstration of the successful operation of a QCL was presented in [1], and was based on a design for an electrically pumped intersubband optical amplifier [2], [3].

Manuscript received ???; revised ???. This work was supported, in part, by the Engineering and Physical Sciences Research Council, UK, and was carried out, in part, by the Jet Propulsion Laboratory, California Institute of Technology under a contract with the National Aeronautics and Space Administration.

J. Green, C. D. Farmer, C. R. Stanley and C. N. Ironside are with the Electronics and Electrical Engineering Department, University of Glasgow, Oakfield Avenue, Glasgow, G12 8LT, UK.

T. B. Boykin is with the Department of Electrical and Computer Engineering, University of Alabama in Huntsville, Huntsville, AL 35899, USA.

M. Garcia is with Thales Research and Technology, 91404 Orsay Cedex, France.

G. Klimeck is with the Jet Propulsion Laboratory, California Institute of Technology, 4800 Oak Grove Drive, MS 169-315 Pasadena, CA 91109-8099, USA.

R. Lake is with the Department of Electrical Engineering, University of California, Riverside, CA 92521-0425, USA.

E-mail: j.green@elec.gla.ac.uk

The main application of QCLs is gas sensing since they have been made to emit at wavelengths in the range of at least $\sim 3.5 \mu\text{m}$ [4] to $\sim 67 \mu\text{m}$ [5], which overlaps the region of the electromagnetic spectrum containing molecular absorption bands. Optimization of the maximum operating temperature, threshold current, output power and careful control of the emission wavelength range are required to exploit fully the capabilities of QCLs in this area. However, the large space available for QCL gain medium design means that an accurate tool is required to select those designs that should be carried forward for expensive and time-consuming growth, fabrication, testing and, ultimately, production.

This paper presents the results of simulations performed using the NanoElectronic MOdeling 3.0.2 software package (NEMO) [6], which is a candidate for such a tool. NEMO was developed by the Applied Research Laboratory of Raytheon TI Systems and others as a comprehensive quantum device modeling package, and is based on the non-equilibrium Green's function formalism. Previously, NEMO has been used for the simulation of resonant tunneling diodes [7]–[9]. Here, one of its sp^3s^* tight-binding models has been used to make predictions of the photon energies, E_{peak} , at which the gain coefficients of several three-well $\text{GaAs}/\text{Al}_x\text{Ga}_{1-x}\text{As}$ QCL gain media are maximized. The predictions are then compared to experimental results.

With a few caveats [10], [11], sp^3s^* tight-binding models offer the possibility of modeling the electronic structure of a III-V heterostructure where transport can take place via any valley. They are also able to model accurately the conduction band non-parabolicity for Γ -like states. Both of these capabilities are potentially important in a QCL, where quantum confinement pushes the resonant states far above the bulk conduction band edge of the well material. The atomic-like basis states used in a tight-binding model should be better suited to modeling the electronic structure of a QCL than the bulk basis states used in a $k \cdot p$ model. The latter set of states should be reserved for modeling heterostructures with layer thicknesses much greater than a monolayer, where the electronic structure is only weakly perturbed from that of the bulk.

II. NOMENCLATURE

Before discussing the simulations, it is necessary to clarify the nomenclature used to describe the electronic resonant

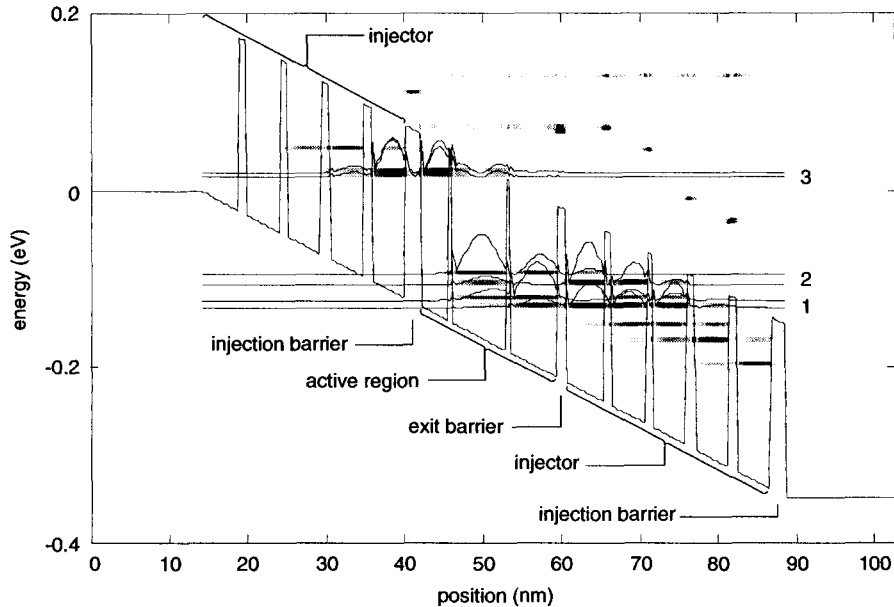


Fig. 1. Resonant states found for the AlAs/GaAs design of Becker *et al.* [12] using a second-nearest neighbor sp^3s^* tight-binding model. The modulus squared of the sum of the tight-binding expansion coefficients for each lattice plane are shown for all the resonant states using gray scale bars and, in addition, for the labeled pairs of states forming levels 1, 2 and 3, with curves. The electric field minimizes the splitting of the two states forming level 3. The bulk conduction band edge energy is also plotted: for the AlAs barriers, this is the bulk X -valley energy.

states in a QCL. The terms level 1, level 2 and level 3 are often used to describe the lowest, second lowest, and third lowest energy resonant states in a biased three-well active region sandwiched not between the injector superlattices of a periodically repeated structure, but barriers that are thick compared with the wave function decay lengths. (The terminology used to describe the various layers in a three-well QCL gain medium is indicated in fig. 1.) The introduction of the proper injection and exit barriers and the injector superlattices on both sides of the active region introduces extra states mostly localized in the injectors, but with some overlap with the active region states. As the electric field applied to the device is altered, these states anti-cross with the states in the active region, causing them to split. The most useful labeling scheme in this more realistic picture, and the one used in this work (see fig. 1), is to assign the terms level 1, 2 and 3 to the anti-crossed *pairs* of states in each active region.

Mid-infrared gain is produced by setting up a population inversion between levels 2 and 3 by engineering the device structure to maximize the non-radiative lifetime of level 3, the stimulated emission rate from level 3 to level 2 and the polar optical phonon scattering rate from level 2 to level 1.

III. METHOD

A. Choice of simulation domain

A QCL gain medium contains typically 25 to 35 repeated stages, each comprising of an injector, an injection barrier, an active region and an exit barrier. It is not feasible or useful to model such a large structure. Instead, the electronic structure of a single stage from an infinitely repeated set of QCL stages was approximated using a biased injector

superlattice / injection barrier / active region / exit barrier / injector superlattice / injection barrier structure, i.e. about one and a half stages. This structure was chosen to model the energies and tight-binding model expansion coefficients of the six states (three pairs) labeled 1, 2 and 3 in fig. 1 accurately. Note that, for states localized close to the edge of the simulation domain, e.g. the lowest energy state shown in fig. 1, the states will only approximate poorly to those in an infinite set of stages. This simulation domain was chosen since, for the structures investigated, level 3 of the active region is split by an interaction with a state mostly localized in just the last two wells of the preceding injector. It is therefore not necessary to include an injection barrier on the upstream side of the simulated domain. An injection barrier is required on the downstream side of the domain since the states in the right-hand injector superlattice that split levels 1 and 2 generally have a significant penetration into the downstream injection barrier. For the unperturbed A1737 design mentioned in fig. 3, the effect of varying the number of layers included in the simulation domain was investigated, and the above choice found to predict the real parts of the eigenenergies satisfactorily.

B. Electronic structure model

A second-nearest neighbor sp^3s^* [13] tight-binding band structure model with spin-orbit coupling and explicit inclusion of up and down spin states was used to model the electronic structure of the lasers. The model parameters, which have not been previously published, are tabulated in table II. These parameters were manually optimized to fit various characteristics of the bulk band structures of the materials to room

TABLE I
THE DESIGNS THAT WERE MODELED, THE REFERENCES THE
EXPERIMENTAL RESULTS WERE TAKEN FROM AND THE TEMPERATURES
AT WHICH THE MEASUREMENTS WERE MADE.

gain medium design	experimental data	temperature (K)
Kruck <i>et al.</i> [15]	[15]	250
Sirtori <i>et al.</i> [16]	[16]	77
A1516 [this paper]	[this paper], [17]	236
A1586 [this paper]	[this paper]	237
Becker <i>et al.</i> [12]	[12]	77

temperature experimental values. The manual optimization was greatly simplified by using the analytic band-edge energy and effective-mass formulae presented in [10]. It is worth drawing attention here to the automatic method presented in [11] for optimizing such parameters, which would greatly reduce the work involved in finding further sets.

The charge on the free carriers and ionized dopant ions in a QCL will affect the energies and wave functions of the resonant states. For these simulations, this effect has been ignored and the electrostatic potential has been assumed to drop linearly across the active region. No scattering self-energies were used and the electronic states are all found for zero in-plane momentum.

C. Threshold electric field determination

The separations in energy of the states forming levels 2 and 3 depend on the externally applied electric field. To find the field at laser threshold rigorously, it would be necessary to evaluate the gain coefficient as a function of electric field, before finding the field that sets the round-trip gain equal to the round-trip loss for a particular waveguide design. For this work, a calculation of the gain coefficient was not made, so two simplified procedures were used to set the electric field. The first procedure involved finding the voltage drop across each structure (to the nearest 0.01 V) that minimized the splitting in energy of level 3. This procedure maximizes the rate at which electrons can tunnel through the injection barrier [2], ensuring that this is not the rate-limiting step for electronic transport. The second procedure minimized the splitting of level 1. There is evidence that tunneling through the exit barrier constitutes a bottleneck for electronic transport in three-quantum well QCLs [14], so this procedure may be more physically realistic than minimizing the splitting of level 3.

D. Simulated designs

To assess the predictions made by NEMO, the designs given in table I were modeled and predictions of the photon energy, E_{peak} , that maximizes the gain coefficient were compared to experimental results. Wafers A1516 and A1586 (see [19] and [20] respectively) were designed and grown at Glasgow University and are based on the design of Kruck *et al.* [15]. A stage from the gain medium in wafer A1516 has layer thicknesses of **51 / 19 / 11 / 56 / **11** / 49 / **28** / 36 / **17** / 32 / 20 / 28 / 22 / 27 / **26** / 27 Å. For A1586, the thicknesses are **51 /****

19 / 11 / 60 / **11 / 49 / **28** / 36 / **17** / 32 / 20 / 28 / 22 / 27 / **26** / 27 Å. For both designs, bold type indicates $Al_{0.33}Ga_{0.77}As$ layers; bold italic type indicates $Al_{0.4}Ga_{0.6}As$; normal type indicates GaAs and the underlined layers are doped with Si to give a sheet doping density of $8.23 \times 10^{12} \text{ cm}^{-2}$ per stage.**

E. Experimental data for comparison

For the design of Kruck *et al.* [15], the experimental E_{peak} was taken from the plot of the electroluminescence spectrum in fig. 2 of [15]. For the design of Sirtori *et al.* [16], the value was taken from the text of [16], which gives the wavelength for single-mode lasing for a Fabry-Perot (FP) device. Their device only lased up to 140 K, and they only quoted an emission wavelength at 77 K, so this value is used here in place of a value for 300 K. The peaks in the gain coefficient for A1516, A1586 and the design of Becker *et al.* [12] were assumed to be at the same photon energies as the peaks of the envelopes of the multi-mode emission intensity spectra of FP lasers. For A1516, the spectra were measured for wet-etched 20 μm by 1.5 mm FP devices using a Bomem DA-3 Fourier transform spectrometer [17]. For A1586, the measurements were made with a Fourier transform spectrometer at Rutherford-Appleton Laboratories on facet-coated [20] 21.4 μm by 0.9 mm FP devices. The value for the design of Becker *et al.* was taken from the caption of fig 2. of [12].

The results in [21] suggest that E_{peak} will decrease by $\sim 4\%$ as the temperature of the active region is changed from 77 K to 300 K, so the lack of room temperature data for some of the designs should not change the qualitative conclusions of this paper.

IV. RESULTS AND DISCUSSION

A. Emission wavelength predictions

The electronic structure for the gain medium design of Becker *et al.* is shown in fig. 1. Explicit calculation of the gain coefficient from the resonant state energies and the tight-binding model expansion coefficients was not implemented for this work, so bounds on the photon energy, E_{peak} , that maximizes the gain coefficient were estimated from just the energies of the states. Different methods were used to find the bounds depending on whether the voltage drop across the simulated region was set to minimize the splitting of level 1 or level 3. If the energies of the two states forming level i are $E_{i,1}$ and $E_{i,2}$, where $E_{i,1} < E_{i,2}$, then, for the voltage drop that minimizes the splitting of level 3, the upper bound on E_{peak} was taken as $(E_{3,1} + E_{3,2})/2 - E_{2,1}$ and the lower bound as $(E_{3,1} + E_{3,2})/2 - E_{2,2}$. This procedure was used since, in a properly designed QCL, the splitting of level 3 is chosen so that the broadening of the levels merges the local density of states of the pair of states into a single peak [22]. For the voltage drop that minimizes the splitting of level 1, the lower bound was taken as $E_{3,1} - E_{2,2}$ and the upper bound as $E_{3,2} - E_{2,1}$.

These bounds are compared with the experimental results in fig. 2. The results show that, for the gain media considered, the two models predict E_{peak} to within at worst 21% of the experimental value. The results do not show that one method

TABLE II
SECOND-NEAREST NEIGHBOR sp^3s^* TIGHT-BINDING MODEL PARAMETERS (IN eV) FOR $Al_xGa_{1-x}As$ AS A FUNCTION OF AL CONTENT, x , USING THE NOTATION OF [10], WHICH IS BASED ON THAT OF [18].

x	0	0.3	0.33	0.4	1
$E_{sa,sa}^{(000)}$	-8.384 280	-8.204 080	-8.174 770	-8.106 370	-7.520 110
$E_{pa,pa}^{(000)}$	0.490 469	0.366 741	0.365 662	0.363 144	0.341 561
$E_{sc,sc}^{(000)}$	-2.758 330	-2.549 170	-2.516 960	-2.441 800	-1.797 610
$E_{pc,pc}^{(000)}$	3.670 470	3.331 270	3.308 640	3.255 850	2.803 310
$E_{s^*a,s^*a}^{(000)}$	8.590 470	8.093 020	8.054 570	7.964 850	7.195 800
$E_{s^*c,s^*c}^{(000)}$	6.720 470	6.341 050	6.314 400	6.252 220	5.719 250
$4E_{sa,sa}^{(\frac{1}{2}\frac{1}{2}\frac{1}{2})}$	-6.460 530	-6.640 000	-6.662 290	-6.714 290	-7.160 000
$4E_{x,x}^{(\frac{1}{2}\frac{1}{2}\frac{1}{2})}$	2.260 950	2.077 870	2.071 960	2.058 170	1.940 000
$4E_{x,y}^{(\frac{1}{2}\frac{1}{2}\frac{1}{2})}$	5.170 000	5.074 000	5.049 400	4.992 000	4.500 000
$4E_{sa,pc}^{(\frac{1}{2}\frac{1}{2}\frac{1}{2})}$	4.680 000	4.900 000	4.907 370	4.924 570	5.072 000
$4E_{sc,pa}^{(\frac{1}{2}\frac{1}{2}\frac{1}{2})}$	8.000 000	8.230 000	8.220 140	8.197 140	8.000 000
$4E_{s^*a,pc}^{(\frac{1}{2}\frac{1}{2}\frac{1}{2})}$	4.650 000	4.239 000	4.197 900	4.102 000	3.280 000
$4E_{pa,s^*c}^{(\frac{1}{2}\frac{1}{2}\frac{1}{2})}$	6.000 000	4.725 000	4.597 500	4.300 000	1.750 000
λ_a	0.140 000	0.140 000	0.140 000	0.140 000	0.140 000
λ_c	0.058 000	0.043 000	0.041 500	0.038 000	0.008 000
$4E_{sa,sa}^{(110)}$	-0.010 000	-0.010 000	-0.010 000	-0.010 000	-0.010 000
$4E_{s^*a,s^*a}^{(110)}$	0.000 000	0.000 000	0.000 000	0.000 000	0.000 000
$4E_{sa,s^*a}^{(110)}$	0.000 000	0.000 000	0.000 000	0.000 000	0.000 000
$4E_{sa,xa}^{(110)}$	0.050 000	0.047 000	0.046 700	0.046 000	0.040 000
$4E_{sa,xa}^{(011)}$	0.058 000	0.052 600	0.052 060	0.050 800	0.040 000
$4E_{s^*a,xa}^{(110)}$	0.020 000	0.020 000	0.020 000	0.020 000	0.020 000
$4E_{s^*a,xa}^{(011)}$	0.040 000	0.058 000	0.059 800	0.064 000	0.100 000
$4E_{xa,xa}^{(110)}$	0.320 000	0.404 660	0.403 470	0.400 694	0.376 900
$4E_{xa,xa}^{(011)}$	-0.050 000	-0.221 180	-0.220 272	-0.218 154	-0.200 000
$4E_{xa,ya}^{(110)}$	1.240 000	1.066 000	1.048 600	1.008 000	0.660 000
$4E_{xa,ya}^{(011)}$	-1.000 000	-1.060 000	-1.066 000	-1.080 000	-1.200 000
$4E_{sc,sc}^{(110)}$	-0.020 000	-0.017 000	-0.016 700	-0.016 000	-0.010 000
$4E_{s^*c,s^*c}^{(110)}$	0.000 000	0.000 000	0.000 000	0.000 000	0.000 000
$4E_{sc,s^*c}^{(110)}$	0.000 000	0.000 000	0.000 000	0.000 000	0.000 000
$4E_{sc,xc}^{(110)}$	0.072 000	0.072 300	0.072 330	0.072 400	0.073 000
$4E_{sc,xc}^{(011)}$	0.020 000	0.026 000	0.026 600	0.028 000	0.040 000
$4E_{s^*c,xc}^{(110)}$	0.010 000	0.016 000	0.016 600	0.018 000	0.030 000
$4E_{s^*c,xc}^{(011)}$	0.093 500	0.074 450	0.072 545	0.068 100	0.030 000
$4E_{xc,xc}^{(110)}$	0.280 000	0.344 600	0.351 061	0.366 136	0.495 350
$4E_{xc,xc}^{(011)}$	-0.100 000	-0.120 080	-0.122 089	-0.126 776	-0.166 950
$4E_{xc,yc}^{(110)}$	0.600 000	0.681 000	0.689 100	0.708 000	0.870 000
$4E_{xc,yc}^{(011)}$	-1.300 000	-1.420 000	-1.453 430	-1.531 430	-2.200 000

for choosing the electric field is any better than the other. The worst-case error could be reduced if a more refined method for predicting the gain spectra was applied to the results of these electronic structure calculations. For example, for the design of Becker *et al.*, the forms of the resonant states in fig. 1 suggest that E_{peak} is closer to the lower bound than the upper bound and, in this case, the lower bound is much closer to the experimental value. Ways in which the model could be improved are given in section VI.

B. Layer thickness rounding

Since NEMO uses a tight-binding model, all layer thicknesses are implicitly rounded to a whole number of monolayers (MLs). This introduces systematic errors into the predictions made by the simulations since all the structures listed in table I were grown with layer thicknesses that are not multiples of the GaAs ML spacing. To investigate the extent to which the rounding might affect the results, three simulations were performed where the layer thicknesses of a gain medium (A1737) were (1) left unchanged, (2) increased by one ML and (3) decreased by one ML. Gain medium A1737 is based on

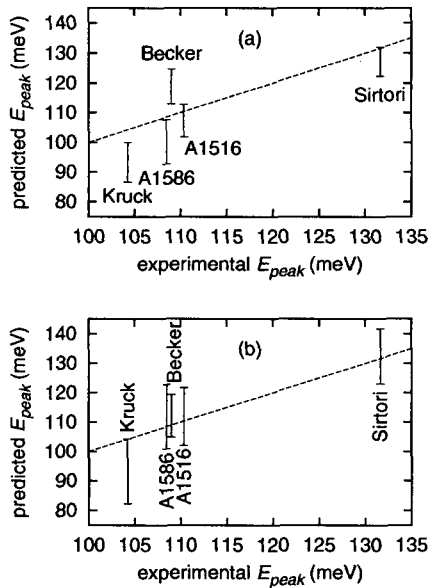


Fig. 2. Comparison of simulation and experimental results for the designs listed in table I. E_{peak} is the photon energy that maximizes the gain coefficient. The straight lines show the ideal case of perfect agreement between the simulated and experimental results. The methods used to find the bounds on the predicted E_{peak} are described in the body of the paper. (a) Voltage drop set to minimize level 3 splitting. (b) Voltage drop set to minimize level 1 splitting.

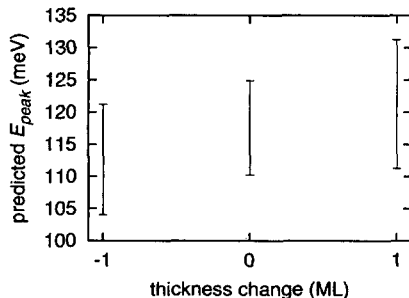


Fig. 3. Predicted bounds on photon energies, E_{peak} , that maximize the gain coefficient for gain medium A1737 and structures formed by increasing/decreasing all layer thickness by one monolayer (ML). The voltage drop across the simulated domain was chosen to minimize the separation of the pair of states forming level 3.

A1586, and has the following layer thicknesses: **16 / 6 / 4 / 21 / 4 / 16 / 10 / 13 / 6 / 11 / 7 / 10 / 8 / 10 / 9 / 10** ML. The same notation used in section III to describe the compositions and doping of A1516 and A1586 has been used here. The sheet doping density per stage was $7.91 \times 10^{12} \text{ cm}^{-2}$. The bounds on E_{peak} for these simulations are presented in fig. 3 and were found by the same procedure used to find the bounds in fig. 2 (a). These results suggest that it is more important to include the injector-induced splittings of levels 2 and 3 in a model that aims to predict E_{peak} than correlated growth thickness errors of ± 1 ML.

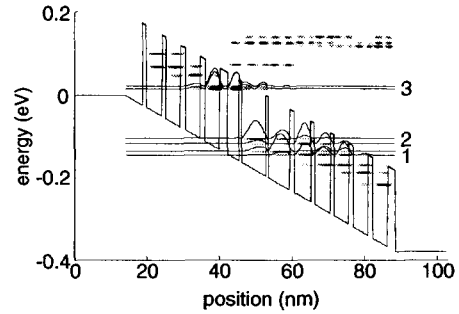


Fig. 4. Resonant states found for the AlAs/GaAs design of Becker *et al.* [12] using a two band $\mathbf{k} \cdot \mathbf{p}$ model. The electric field minimizes the splitting of the states forming level 3. The bulk conduction band edge energy is also plotted: for the AlAs barriers, this is the bulk X -valley energy.

C. Other systematic errors

Further systematic errors in the model might include: the neglect of the excitation of charge carriers to finite in-plane momenta at finite temperature and the resulting non-parabolicity induced wavelength shift [21]; the neglect of the Hartree potential and the choice of the tight-binding model's Hamiltonian matrix elements.

D. Comparison with empirical two-band $\mathbf{k} \cdot \mathbf{p}$ model

The two-band empirical $\mathbf{k} \cdot \mathbf{p}$ model [23] is used by many groups to predict the state separations in QCLs with reasonable accuracy: e.g. for the design of Becker *et al.*, [12] used this model to predict a value of 109 meV for E_{peak} , which, to three significant figures, was identical to their experimental value at 77 K. The main advantage that the model presented here has over the two-band empirical $\mathbf{k} \cdot \mathbf{p}$ model is its ability to model the X -like states directly. These states, which are all localized within the barriers, are present in fig. 1, but are absent in fig. 4, where the calculation for the design of Becker *et al.* was repeated using NEMO's two-band $\mathbf{k} \cdot \mathbf{p}$ model. (It can also be seen that there are some above-barrier resonances in fig. 4 that are not present in fig. 1. This is an artifact of the numerical method used to resolve the resonant states.)

The empirical two-band model only has $n + 1$ adjustable parameters for an n material heterostructure e.g. for a single material, the bulk imaginary dispersion relation cannot be set independently of the effective mass and non-parabolicity parameters and for two materials, the non-parabolicity parameter can only be set for one of the materials. The sp^3s^* tight-binding model used in this work has 37 parameters per material, providing for better modeling of the detailed alignment between the resonant states in each active region and its neighboring injector superlattices.

E. InP system

NEMO has also been used to predict E_{peak} with reasonable accuracy for $\text{In}_{0.53}\text{Ga}_{0.47}\text{As} / \text{In}_{0.52}\text{Al}_{0.48}\text{As}$ QCLs, although the results are not shown or considered further here. The non-parabolicity in this system is even more pronounced than for the $\text{Al}_x\text{Ga}_{1-x}\text{As}$ system.

V. CONCLUSION

NEMO has been shown to be capable of predicting the photon energy, E_{peak} , at the peak in the gain coefficient spectrum of various quantum cascade laser gain medium designs to within at worst 21% of the experimental value. It is anticipated that the accuracy of the predictions can be improved by refining the method used to model the gain spectra. The sp^3s^* tight-binding model used by NEMO is not only capable of predicting the resonant state separations, but can also directly model the X-like states. Finally, it has been shown that correlated errors in the layer thicknesses of ± 1 ML and the procedure used to set the electric field across the device are less important when determining E_{peak} than the injector-induced splittings of levels 2 and 3.

VI. FUTURE WORK

To carry this work forward, it will be necessary to calculate the gain coefficient, taking into account the injector-induced splitting of levels 2 and 3, to predict a single value for E_{peak} and not just bounds. This will require NEMO to be modified so that it can calculate the polar optical phonon (POP) and optical stimulated emission scattering rates between resonant states found using its ten-band sp^3s^* models. Ideally, the e-POP scattering rates should be found using the dielectric continuum model for phonons in a heterostructure, since modeling the scattering of electrons in QCLs using bulk phonons has been found to be inadequate [24]. Advantage should also be taken of NEMO's abilities to model properly the electronic structure of states with X-like character and to model InP-system QCLs. Self-consistent inclusion of quantum mechanical charge via the Hartree approximation would be a useful feature to add to the model, as would the ability to include strained layers [4] and carrier-carrier scattering rates [25].

In conclusion, NEMO has been shown to be capable of analyzing existing QCL gain medium designs. It now needs to be shown that it can be used as an efficient and accurate design tool.

ACKNOWLEDGMENT

Thanks are due to John R. Barker at the University of Glasgow for establishing contact with the NEMO team at JPL and UC Riverside. Thanks must also go to Fabiano Oyafuso at JPL and John H. Davies at the University of Glasgow for discussions related to this work and to Erwan Normand at Strathclyde University for performing spectral measurements on devices fabricated from wafers A1516 and A1586. This NEMO related work serves the on-going JPL efforts on the development of far-infrared sensors and lasers.

REFERENCES

- [1] J. Faist, F. Capasso, D. L. Sivco, C. Sirtori, A. L. Hutchinson, and A. Y. Cho, "Quantum cascade laser," *Science*, vol. 264, pp. 553–556, 1994.
- [2] R. F. Kazarinov and R. Suris, "Possibility of the amplification of electromagnetic waves in a semiconductor with a superlattice," *Sov. Phys. Semicond.*, vol. 5, pp. 707–709, 1971.
- [3] —, "Electric and electromagnetic properties of semiconductors with a superlattice," *Sov. Phys. Semicond.*, vol. 6, pp. 120–131, 1972.
- [4] J. Faist, F. Capasso, D. L. Sivco, A. L. Hutchinson, S.-N. G. Chu, and A. Y. Cho., "Short wavelength ($\lambda \sim 3.4\mu\text{m}$) quantum cascade laser based on strained (*sic*) compensated InGaAs/AlInAs," *Appl. Phys. Lett.*, vol. 72, pp. 680–682, 1998.
- [5] R. Köhler, A. Tredicucci, F. Beltram, H. E. Beere, E. H. Linfield, A. G. Davies, D. A. Ritchie, S. S. Dhillon, and C. Sirtori, "High-performance continuous-wave operation of superlattice terahertz quantum-cascade lasers," *Appl. Phys. Lett.*, vol. 82, pp. 1518–1520, 2003.
- [6] Nemo home page. [Online]. Available: <http://www-hpc.jpl.nasa.gov/PEP/gecko/nemo>
- [7] G. Klimeck, R. Lake, R. C. Bowen, W. R. Frensley, and T. S. Moisea, "Quantum device simulation with a generalized tunneling formula," *Appl. Phys. Lett.*, vol. 67, pp. 2539–2541, 1995.
- [8] R. Lake, G. Klimeck, R. C. Bowen, and D. Jovanovic, "Single and multiband modeling of quantum electron transport through layered semiconductor devices," *Appl. Phys. Lett.*, vol. 81, pp. 7845–7869, 1997.
- [9] G. Klimeck, "Indirect bandgap-like current flow in direct bandgap electron resonant tunneling diodes," *Phys. Stat. Sol. (b)*, vol. 226, pp. 9–19, 2001.
- [10] T. B. Boykin, "Improved fits of the effective masses at Γ in the spin-orbit, second-nearest-neighbor sp^3s^* model: Results from analytic expressions," *Phys. Rev. B*, vol. 56, pp. 9613–9618, 1997.
- [11] G. Klimeck, R. C. Bowen, T. B. Boykin, C. Salazar-Lazaro, T. A. Cwik, and A. Stoica., "Si tight-binding parameters from genetic algorithm fitting," *Superlattices and Microstructures*, vol. 27, pp. 77–88, 2000.
- [12] C. Becker, C. Sirtori, H. Page, G. Glastre, V. Ortiz, X. Marcadet, M. Stellmacher, and J. Nagle, "AlAs/GaAs quantum cascade lasers based on large direct conduction band discontinuity," *Appl. Phys. Lett.*, vol. 77, pp. 463–465, 2000.
- [13] P. Vogl, H. P. Hjalmarson, and J. D. Dow, "A semi-empirical tight-binding theory of the electronic structure of semiconductors," *J. Phys. Chem. Solids*, vol. 44, pp. 365–378, 1983.
- [14] J. Faist, D. Hofstetter, M. Beck, T. Aellen, M. Rochat, and S. Blaser, "Bound-to-continuum and two-phonon resonance quantum-cascade lasers for high duty cycle, high-temperature operation," *IEEE J. Quantum Electron.*, vol. 38, pp. 533–546, 2002.
- [15] P. Kruck, H. Page, C. Sirtori, S. Barbieri, M. Stellmacher, and J. Nagle., "Improved temperature performance of $\text{Al}_{0.33}\text{Ga}_{0.67}\text{As}/\text{GaAs}$ quantum-cascade lasers with emission wavelength at $\lambda \sim 11\mu\text{m}$," *Appl. Phys. Lett.*, vol. 76, pp. 3340–3342, 2000.
- [16] C. Sirtori, P. Kruck, S. Barbieri, P. Collot, J. Nagle, M. Beck, J. Faist, and U. Oesterle., "GaAs/Al_xGa_{1-x}As quantum cascade lasers," *Appl. Phys. Lett.*, vol. 73, pp. 3486–3488, 1998.
- [17] M. Garcia, E. Normand, C. R. Stanley, C. N. Ironside, C. D. Farmer, G. Duxbury, and N. Langford, "Spectroscopy of NH_3 with an AlGaAs-GaAs quantum cascade laser operating with a thermoelectric cooler." Submitted to *Optics Comms*.
- [18] J. C. Slater and G. F. Koster, "Simplified LCAO method for the periodic potential problem," *Phys. Rev.*, vol. 94, pp. 1498–1524, 1954.
- [19] M. Garcia, C. Farmer, C. N. Ironside, and C. Stanley, "GaAs-AlGaAs quantum cascade laser at $\lambda \approx 10.5\mu\text{m}$ working above zero degree Celsius," *Quantum Electronics and Photonics 15*, poster P2-3, 2001.
- [20] C. D. Farmer, C. R. Stanley, C. N. Ironside, and M. Garcia., "Improved GaAs-based quantum cascade laser ($\lambda \sim 11\mu\text{m}$) using a high-reflectivity metal facet coating," *Electron. Lett.*, vol. 38, pp. 1443–1444, 2002.
- [21] Y. B. Li, J. W. Cockburn, M. S. Skolnick, J. P. Duck, M. J. Birkett, I. A. Larkin, R. Grey, G. Hill, and M. Hopkinson., "Mid-infrared intersubband electroluminescence from a single-period GaAs/AlGaAs triple barrier structure," *Appl. Phys. Lett.*, vol. 72, pp. 2141–2143, 1998.
- [22] C. Sirtori, F. Capasso, J. Faist, A. L. Hutchinson, D. L. Sivco, and A. Y. Cho., "Resonant tunneling in quantum cascade lasers," *IEEE J. Quantum Electron.*, vol. 34, pp. 1722–1729, 1998.
- [23] D. F. Nelson, R. C. Miller, and D. A. Kleinman., "Band nonparabolicity effects in semiconductor quantum wells," *Phys. Rev. B*, vol. 35, pp. 7770–7773, 1987.
- [24] C. Sirtori, H. Page, C. Becker, and V. Ortiz, "GaAs-AlGaAs quantum cascade lasers: Physics, technology, and prospects," *IEEE J. Quantum Electron.*, vol. 38, pp. 547–558, 2002.
- [25] M. Rochat, L. Ajili, H. Willenberg, J. Faist, H. Beere, G. Davies, E. Linfield, and D. Ritchie, "Low-threshold terahertz quantum-cascade lasers," *Appl. Phys. Lett.*, vol. 81, pp. 1381–1383, 2002.



Jeremy Green read Natural Sciences at Pembroke College, University of Cambridge, UK from 1995 to 1999. These four years included courses on Materials Science, Physics, Mathematics, Computer Science and French, and lead to the awards of BA Hons. Natural Sciences and M.Sci. Materials Science and Metallurgy, as well as two college examination prizes. He is currently a Ph.D. student working on a project entitled, "Quantum Cascade Lasers for Gas Sensing" in the Molecular Beam Epitaxy and Optoelectronics groups at the Department of Electronics and Electrical Engineering, University of Glasgow, UK.

During his Ph.D., he has been employed as a Research Assistant as part of an European Office of Aerospace Research and Development funded contract.



Timothy B. Boykin Timothy B. Boykin was born in Houston, Texas, USA in 1964. He received the B.S. in electrical engineering *summa cum laude* from Rice University in 1987, and the M.S. and Ph.D. in electrical engineering from Stanford University in 1988 and 1992, respectively. His dissertation research introduced the first numerically-stable multi-band tight-binding calculation of RTD I - V characteristics. He joined the Department of Electrical and Computer Engineering of the University of Alabama in Huntsville in 1992 as an Assistant Professor and

is currently Associate Professor. His work has concentrated on full-band structure models for nano-devices, including complex band structure methods, properties of tight-binding models, the effect of in-plane wave vector on tunneling, and modeling electromagnetic interactions in tight-binding models. Several of these models and methods have been incorporated into NEMO due to his frequent collaborations with Gerhard Klimeck and Roger Lake. He has authored or co-authored over 40 journal articles. He is currently researching full-band structure models for quantum dots.

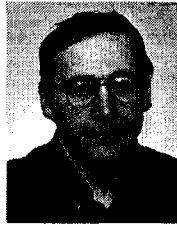


Corrie D. Farmer has spent eleven years at the University of Glasgow, in which time he has completed a European Master of Engineering (M.Eng.) degree in electronics, a Ph.D. and has held three research assistant (RA) positions. Working at GEEO in Grenoble, France for six months as part of his M.Eng. course, he helped develop a fiber optic-based temperature sensor. During his Ph.D., he designed, fabricated and evaluated InP-based Quantum Cascade Lasers (QCLs), and was the first person to demonstrate a QCL in the UK. He then joined the

EU funded Superior Semiconductor Mid-Infrared Lasers (SUPERSMILE) consortium, in which he concentrated on the design and fabrication of low-threshold GaAs-based QCLs using integrated photonic band gap (PBG) structures and high reflectivity (HR) coatings. Following on from encouraging preliminary research, he is currently the principal investigator and RA on a Proof of Concept project funded by Scottish Enterprise, with the aim of developing and commercializing an improved oxidation process for InP-based III-V materials and devices.



Michel Garcia Biography to be supplied later.

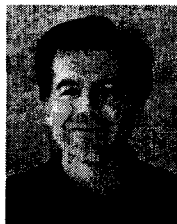


Charles N. Ironside was born in Aberdeen, Scotland, UK. He received the B.Sc. degree (first-class honors) in physics in 1974, and the Ph.D. degree in 1978, both from Heriot-Watt University, Edinburgh, UK. His Ph.D. work involved the Spin-Flip Raman Laser, a type of tunable semiconductor laser. From 1978 to 1984, he was a post-doctoral Research Assistant at the University of Oxford, Oxford, UK, first with the Inorganic Chemistry Department, working on time-resolved spectroscopy of solids and energy-transfer mechanisms between luminescent ions, and then with the Clarendon Laboratory, working on time-resolved spectroscopy of solids on a picosecond timescale and ultrafast effects in semiconductors. In 1984, he moved to the Department of Electronics and Electrical Engineering, University of Glasgow, Glasgow, UK. He has published more than 150 research papers. His current research interests include ultrafast all-optical switching in semiconductor waveguides, monolithic mode locking of semiconductor lasers, ultrafast optoelectronic modulators employing resonant tunneling diodes and quantum-cascade lasers.



Gerhard Klimeck is the technical group supervisor of the Applied Cluster Computing Technologies Group since April 2002 and a Principal member at the NASA Jet Propulsion Laboratory since September 2001. He joined JPL in February 1998 as a Senior member technical staff. His research interest is in the quantum mechanical modeling of electron transport through nanoelectronic devices, parallel cluster computing, genetic algorithms, and parallel image processing. At JPL, he has utilized technology in these areas to explore the nanoelectronic design

space and has developed the 3-D Nanoelectronic Modeling tool (NEMO 3-D) that enables the analysis of electronic structure in systems containing as many as 32 million atoms. He continues to expand NEMO 1-D to study hole transport, optical devices and spintronic devices. His work on mars image processing enabled the integration of parallel processing algorithms in the MIPL data analysis pipeline. Previously, he was a member of technical staff at the Central Research Lab. of Texas Instruments (which transitioned to the Applied Research Laboratory of Raytheon), where he served as manager and principal architect of the Nanoelectronic Modeling (NEMO) program. Dr. Klimeck received his Ph.D. in 1994 from Purdue University, where he studied electron transport through quantum dots, resonant tunneling diodes and 2-D electron gases. His research for his German electrical engineering degree, which he obtained in 1990 from Ruhr-University Bochum, concerned the study of laser noise propagation. Dr. Klimeck's work is documented in over 75 peer reviewed publications and over 120 conference presentations. These publications are cited by other authors over 300 times. He is a member of IEEE, APS, HKN and TBP.



Roger Lake received his Ph.D. in electrical engineering from Purdue University in 1992 and joined the Nanoelectronics Branch of Central Research Labs., Texas Instruments in Dallas in 1993 to develop the theory for the Nanotechnology Engineering Program which became known as NEMO. In 1997, the Nanoelectronics Branch was acquired by Raytheon, where Lake worked on a number of different materials and devices: Si/SiGe tunnel diodes, InGaAs/InAlAs HEMTs for both high speed ADCs and low power memory, InAs/AlSb and In-

GaAs/InAs/AlAs RTDs for for ADC, TSRAM, and THz applications. Currently, Lake is in the Electrical Engineering Department of the University of California, Riverside working on full-band, 3D modeling of Si/SiGe quantum confined structures, high frequency response of RTDs, molecular electronics, and quantum computing.



Colin R. Stanley received the first-class honors degree in electronic engineering from the University of Sheffield, Sheffield, UK, in 1966, and the Ph.D. degree (for research into the nonlinear optical properties of tellurium) from the University of Southampton, Southampton, UK, in 1970. From 1970 to 1972, he was an ICI Research Fellow at the University of Southampton, continuing work on optical parametric amplifiers and oscillators. He spent part of 1971 at the Centre Nationale d'Études des Télécommunications, Bagneux, Paris, France, as

a Visiting Scientist. He joined the Department of Electronics and Electrical Engineering, University of Glasgow, Glasgow, Scotland, in 1972 as a Research Fellow, and was subsequently appointed Lecturer (1974), Senior Lecturer (1982), Reader (1989), and Titular Professor (1992). He was a Visiting Scientist at Cornell University, Ithaca, NY, during 1982, and spent six months during 1997-1998 on industrial secondment with Motorola, East Kilbride, under a scheme financed by the Royal Academy of Engineering. He has been author or co-author of over 130 papers on molecular beam epitaxy (MBE) and related topics. Dr. Stanley is a member of the IEEE, the Institution of Electrical Engineers and the Institute of Physics.